Biocatalysis and Agricultural Biotechnology 18 (2019) 101086

Contents lists available at ScienceDirect

Biocatalysis and Agricultural Biotechnology

journal homepage: www.elsevier.com/locate/bab

Invivo, molecular docking, spectroscopy studies of (S)-2,3-Dihydro-5,7-dihydroxy-2(3-hydroxy-4-methoxyphenyl)-4H-1-benzopyran-4-one: A potential uptake PI3/AKT inhibitor

M. Govindammal[a], M. Prasath[a,*], S. Kamaraj[b], B. Sathya[a]

[a] Department of Physics, Periyar University PG Extension Centre, Dharmapuri, 636701, India
[b] Department of Biotechnology, Periyar University PG Extension Centre, Dharmapuri, 636701, India

ARTICLE INFO

Keywords:
Lung cancer
Molecular docking
Fukui function
Hesperetin and PI3K/AKT

ABSTRACT

The molecule (S)-2,3-Dihydro-5,7-dihydroxy-2(3-hydroxy-4-methoxyphenyl)-4H-1-benzopyran-4-one (Hesperetin) was optimized utilizing density functional theory (DFT) with B3LYP/6-311G(d,p) basis set. The vibrational frequencies and potential energy distribution (PED)% of Hesperetin molecule was computed and it shows good agreement with the experimental values. The reactivity nature of the molecule was analysed with various DFT methods such as local reactivity descriptors, Molecular Electrostatic Potential (MEP) and Frontier Molecular orbitals (FMOs). Drug likeness and ADMET properties were analysed for the prediction of pharmacokinetic properties like Absorption, Distribution, Metabolism, Excretion and Toxicity. The molecular docking analysis reveals that inhibitory nature of the Hesperetin molecule. Various signalling pathways are regulating the lung cancer progression including PI3K/AKT. Interrupting this signalling pathway could help us discover the new drug derivatives. Hence, the present study reports the structural details, intermolecular interactions of PI3K and Hesperetin and the toxicity study (*in vivo*) was also analysed by inhibition of human lung cancer cells (A549) proliferation.

1. Introduction

Lung cancer is the most common cancer throughout the world and is the leading cause of cancer transience (Jemal et al., 2011). The (S)-2,3-Dihydro-5,7-dihydroxy-2(3-hydroxy-4-methoxyphenyl)-4H-1-benzopyran-4-one molecule is chosen as the Non-Small Cell Lung Cancer (NSCLC) agent. Hesperetin is the 4′-methoxy derivative of eriodictyol, a flavanone. Hesperetin is a naturally occurring flavanone-glycoside, the main flavonoid in lemon and sweet orange (Lewinsohn et al., 1989). Hesperetin is also known as 3′, 5, 7-trihydroxy-4-methoxy flavanone ($C_{16}H_{14}O_6$), is a member of the flavanone subclass of flavonoids. Hesperetin is predominantly metabolized to hesperetin-7-O-β-Dglucuronide (H7-OG) and hesperetin-3′-O-β-D-glucuronide (H3′-OG). Akt, together with phosphatidyl inositol 3-kinase(PI3K), are the key elements of the Akt signalling cascade, also known as PI3K/Akt, this signal transduction path stimulates the survival and growth in response to extracellular signals (Arcaro and Guerreiro, 2007). Akt is also activated in variety of human cancers, including lungs, breast, ovarian, gastric and pancreatic carcinomas (Shi.Y & Lasko, L. et al., 2005).

Phosphatidylinositol-3 Kinase (PI3K) and serine-threonine protein Kinase AKT (also known as protein Kinase B) seems to make immune cell activation by regulation of the key inflammatory cytokines (Weichhart, T et al., 2008), changes in PI3K/AKT signalling pathway may contribute to specific therapeutic effects for the cancer. In addition, the physiological function of PTEN is to dephosphorylate the second messengers generated by the activation of PI3K, thereby downregulates or terminates insulin signalling downstream of PI3K (Peyrou,U., 2010).

The PI3K and Akt pathway (Burgering, B. M., 1995;Liu, W., 1999; Muthuswamy, S. K. et al., 1999) are two major signalling routes for the ErbB family, including EGFR. These pathways regulate multiple biological process, such as gene expression, cellular proliferation, angiogenesis, and inhibition of apoptosis, which subscribes to the development of malignancy (Chan, T. O. et al., 1999). In the present work, the most secure optimized molecular structure of Hesperetin was calculated. The elaborate vibrational spectral analysis was performed by experimental and theoretical methods. The calculated vibrational wavenumber has been assigned with potential energy distribution (PED). Fukui function was carried out to identify the reactive sites of the molecule. Frontier molecular orbitals (FMOs) analyses were performed.

* Corresponding author.
E-mail address: drprasath@periyaruniversity.ac.in (M. Prasath).

https://doi.org/10.1016/j.bcab.2019.101086
Received 7 November 2018; Received in revised form 25 February 2019; Accepted 7 March 2019
Available online 11 March 2019
1878-8181/

Table 1
Optimized geometrical parameters bond length, bond angle of Hesperetin B3LYP/6- 311G(d,p) in comparison with experimental data.

Parameters	Experimental	Theoretical	Parameters	Experimental	Theoretical
Bond length (Å)					
C(1)-C(2)	1.481	1.533	C(13)-C(14)-C(15)	122.0	120.2
C(1)-O(6)	1.442	1.487	C(13)-C(14)-O(20)	118.7	119.8
C(1)-C(12)	1.512	1.506	C(15)-C(14)-O(20)	119.4	119.8
C(2)-C(3)	1.504	1.512	C(14)-C(15)-C(16)	120.3	120.0
C(3)-C(4)	1.430	1.442	C(14)-C(15)-O(18)	117.6	113.3
C(3)-O(11)	1.231	1.268	C(16)-C(15)-O(18)	125.4	126.3
C(4)-C(5)	1.406	1.417	C(15)-O(18)-C(19)	117.7	119.0
C(4)-C(10)	1.406	1.428	C(2)-C(1)-C(12)	114.6	114.3
C(5)-O(6)	1.361	1.388	C(1)-C(12)-C(13)	120.9	120.4
C(5)-C(7)	1.377	1.386	C(9)-C(10)-O(22)	118.8	118.4
C(7)-C(8)	1.384	1.403	C(9)-C(8)-O(21)	120.7	116.4
C(8)-C(9)	1.343	1.394	C(7)-C(8)-O(21)	118.0	121.4
C(8)-O(21)	1.410	1.384	C(3)-C(4)-O(11)	123.3	122.5
C(9)-C(10)	1.373	1.390	C(12)-C(13)-C(14)	120.0	119.9
C(10)-O(22)	1.361	1.361	C(13)-C(12)-C(17)	117.7	119.5
C(12)-C(13)	1.389	1.404	C(15)-C(16)-C(17)	120.4	119.2
C(12)-C(17)	1.381	1.397	C(1)-C(12)-C(17)	121.2	119.9
C(13)-C(14)	1.375	1.385	C(10)-C(4)-C(8)	118.5	120.0
C(14)-C(15)	1.406	1.390	C(9)-C(10)-C(4)	122.0	120.8
C(14)-O(20)	1.322	1.385	C(9)-C(8)-C(7)	121.3	121.4
C(15)-C(16)	1.381	1.389	C(8)-C(7)-C(5)	118.7	118.4
C(15)-O(18)	1.352	1.399	C(4)-C(10)-O(22)	119.2	120.6
C(16)-C(17)	1.372	1.402	C(12)-C(17)-C(16)	122.2	120.6
O(18)-C(19)	1.475	1.452			
Bond Angle (°)			Torsion angle (°)		
C(2)-C(1)-O(6)	112.1	109.5			
C(2)-C(1)-C(12)	114.6	109.5	C(5)-O(6)-C(1)-C(2)	52.6	50.3
O(6)-C(1)-C(12)	107.0	107.5	O(6)-C(1)-C(2)-C(3)	−52.3	−53.9
C(1)-C(2)-C(3)	111.6	111.6	C(1)-C(2)-C(3)-C(4)	25.4	31.2
C(2)-C(3)-C(4)	116.0	117.0	C(2)-C(3)-C(4)-C(5)	2.4	−1.7
C(2)-C(3)-O(11)	120.7	120.3	O(6)-C(5)-C(4)-C(3)	−4.1	−4.2
C(4)-C(3)-O(11)	123.3	122.5	C(1)-O(6)-C(5)-C(4)	−23.9	−21.7
C(3)-C(4)-C(5)	121.4	120.0	O(6)-C(1)-C(12)-C(13)	27.4	- 44.7
C(3)-C(4)-C(10)	121.2	121.4	C(2)-C(1)-C(12)-C(17)	−33.5	−101.4
C(5)-C(4)-C(10)	117.3	117.8			
C(4)-C(5)-O(6)	120.0	120.0			
C(4)-C(5)-C(7)	122.2	121.6			
O(6)-C(5)-C(7)	117.2	117.0			
C(1)-O(6)-C(5)	115.1	116.5			

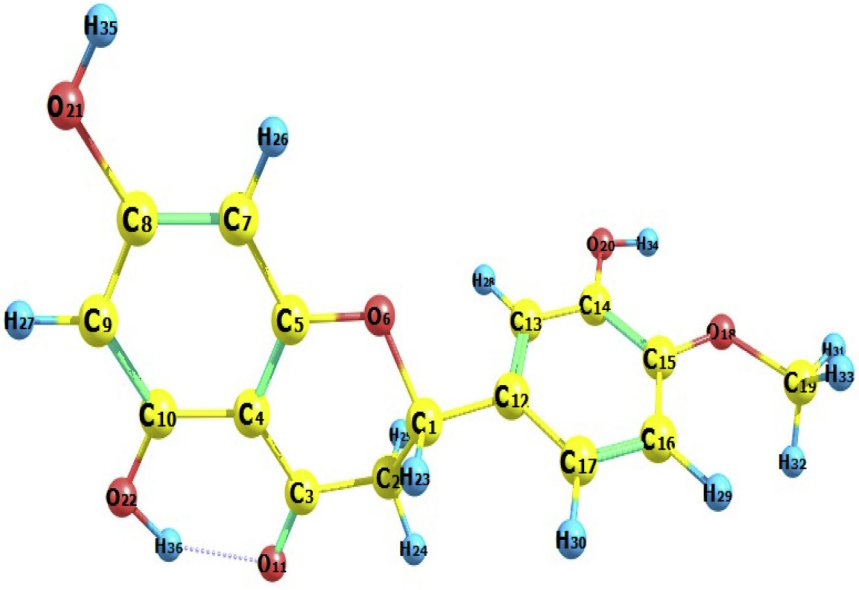

Fig. 1. Optimized geometric structure with atoms numbering of Hesperetin.

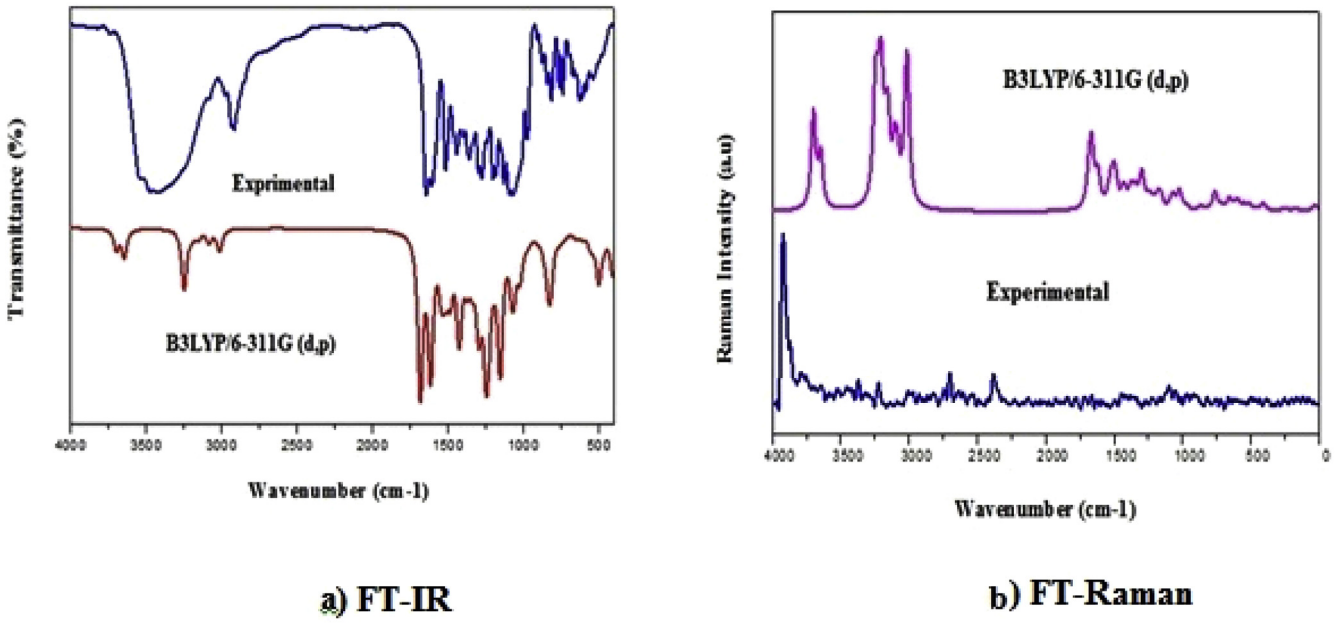

Fig. 2. a) FT-IR and b) FT-Raman Spectra of Hesperetin (Experimental and B3LYP/6-311G (d,p)).

Molecular electrostatic potential (MEP) surface was simulated and visualized. The molecular orbital contributions were investigated by using the total density of states (TDOS). The thermodynamic properties of the Hesperetin molecule were calculated at different temperatures, revealing the correlation between heat capacity (C), enthalpy (H) and entropy (S) with temperatures. Docking of small molecule (ligand) in the receptor binding site (targeted protein) and computation of binding affinity of the stable complex is the major tool in structure-based computer-assisted drug design. Molecular docking concludes the target binding site of the ligand molecule.

2. Materials and methods

2.1. Chemicals

Dulbecco's Modified Eagle's Medium (DMEM), 0.25% trypsin-EDTA solution, sodium bicarbonate solution, bovine serum albumin (BSA), 3-[4,5-dimethythiazol-2-yl] 2,5-diphenyl tetrazolium bromide (MTT), ethidium bromide, acridine orange and Hesperetin were purchased from Sigma Chemicals Co. (St. Louis, MO, USA). Fetal Bovine Serum (FBS) and antibiotic/antimycotic solution were purchased from Gibco (Gibco, USA).

2.2. Cell culture

The A549 cell line was procured from the National Centre for Cell Science (Pune, India). Cells were grown in T75 culture flasks containing DMEM supplemented with 10% FBS at 37 °C in humidified air with 5% CO_2. Upon reaching confluence, cells were detached using Trypsin-EDTA solution.

2.3. Viability assay

The inhibitory effect of Hesperetin on the growth of A549 cells was measured by MTT assay as described. The cells were dispensed in 24 well plates at a density of 5×10^4 cells per well. After 12hrs of incubation, they were treated with various concentrations of Hesperetin for the indicated time periods. At the end of treatment, media which were in control and Hesperetin treated cells were discarded and 500 µl of MTT containing DMEM (0.5 mg/ml) was added to each well. MTT containing medium was then discarded and the cells were washed with 1x phosphate buffered saline (PBS; 1 ml). Crystals were then dissolved by adding 500 µl of solubilization solution and was mixed effectively by pipetting up and down. Spectrophotometrical absorbance of the purple blue formazan dye was measured using a micro plate reader at 620 nm. The optical density of each sample was then compared with control optical density and graphs were plotted. Based on MTT assay, doses were selected as 12.5 µM Hesperetin treatment for 24 hrs of further studies because these are doses below IC_{50} (50% inhibitory concentration) value of Hesperetin in A549 cells.

Viability (%) = 100-[(A620, control-A620, Hesperetin)/A620, control x100].

2.4. Ethidium bromide/acridine orange (dual staining)

Ethidium bromide/acridine orange staining was carried out by the method of Gohel et al. A549 cells were plated at a density of 5×10^4 in 6 well plates containing sterile coverslips. They were allowed to grow at 37 °C in a humidified CO_2 incubator until they were 70–80% confluent. Then cells were treated with Hesperetin (12.5 µM) for 24 hrs. The culture medium was aspirated from each well and the cells were gently rinsed twice with PBS at room temperature. Then the cover slips were taken and put on glass slides to be stained with 100 µl of dye mixture (1:1 of ethidium bromide and acridine orange) and were viewed immediately by fluorescence microscopy. Viable cells had green fluorescent nuclei with organized structure, early apoptotic cells had yellow chromatin in nuclei that were highly condensed or fragmented; apoptotic cells also exhibited membrane blebbing. Late apoptotic cells had orange chromatin with nuclei that were highly condensed and fragmented; necrotic cells had bright orange chromatin in round nuclei. Only cells with yellow, condensed, or fragmented nuclei were counted as apoptotic cells in a blinded, unbiased manner. For each sample, at least 500 cells/well and 4 wells/condition were counted, and the percentage of apoptotic cells was determined [% of apoptotic cells = (total number of apoptotic cells/total number of cells counted) x100].

3. Experimental details

The FT-IR spectrum of Hesperetin was recorded in the region 4000 to 400 cm^{-1} on IFS 66V spectrophotometer using KBr pellet technique.

Table 2
Observed and calculated vibrational frequency of Hesperetin at B3LYP method with 6-311G (d,P) basis set.

Mode No	Experimental wave number (cm-1)		Theoretical wave number (cm-1)		IR intensities		RAMAN intensities		Assignments PED
	FTIR	FT RAMAN	Unscaled frequency	Scaled frequency	Rel	Abs	Rel	Abs	
W(102)	3427		3699	3558	68	13	178	100	νOH(100)
W(101)		3501	3646	3508	96	18	96	54	νOH(100)
W(100)			3250	3126	200	38	88	50	νOH(99)
W(99)		3104	3240	3117	2	0	130	73	νCH(100)
W(98)			3218	3096	0	0	80	45	νCH(100)
W(97)			3205	3083	14	3	104	58	νCH(93)
W(96)	3061		3201	3079	3	1	81	45	νCH(93)
W(95)			3172	3052	11	2	55	31	νCH(88)
W(94)	3027	3032	3154	3034	21	4	132	74	νCH(94)
W(93)		2900	3103	2986	6	1	84	47	νCH(93)
W(92)			3084	2967	37	7	60	34	νCH(100)
W(91)	2918	2912	3030	2915	13	2	39	22	νCH(93)
W(90)			3014	2899	18	3	149	84	νCH(91)
W(89)		2898	3013	2898	47	9	113	64	νCH(96)
W(88)	1646	1617	1685	1621	532	100	48	27	νOC(74)
W(87)	1609		1665	1602	5	1	110	62	νCC(23)
W(86)			1629	1567	32	6	17	10	νCC(47)
W(85)			1619	1557	193	36	11	6	νCC(22)
W(84)	1518	1563	1614	1553	241	45	37	21	νCC(40)
W(83)		1485	1549	1490	89	17	5	3	νCC(24)
W(82)		1475	1540	1481	86	16	8	4	νCC(40)
W(81)		1464	1526	1468	12	2	26	14	νCC(42)
W(80)		1454	1516	1458	104	20	17	10	νCC(22)
W(79)	1444		1504	1447	14	3	29	16	νCC(16)
W(78)			1491	1435	28	5	21	12	νCC(29)
W(77)			1491	1434	21	4	10	6	νOC(14)
W(76)	1402		1483	1427	105	20	14	8	νCC(24)
W(75)		1380	1434	1380	180	34	23	13	νOC(33)
W(74)	1361	1363	1422	1368	174	33	15	9	νOC(25)
W(73)			1391	1339	22	4	5	3	νOC(32)
W(72)			1379	1326	67	13	23	13	νOC(132)
W(71)		1301	1365	1313	53	10	12	7	νCC(16)
W(70)	1294	1291	1344	1293	43	8	20	11	νCC(22)
W(69)			1339	1288	52	10	6	4	νOC(59)
W(68)		1311	1311	1261	52	10	6	3	νOC(47)
W(67)			1301	1252	75	14	20	11	νOC (20)
W(66)			1294	1245	169	32	42	23	νOC (12)
W(65)			1258	1211	49	9	10	6	νOC (41)
W(64)	1204		1250	1203	299	56	1	1	νOC (37)
W(63)		1187	1235	1188	136	26	12	7	νOC (59)
W(62)	1184	1169	1232	1185	73	14	4	2	νOC (26)
W(61)			1208	1162	22	4	6	3	νOC (45)
W(60)			1197	1152	28	5	4	2	νOC (50)
W(59)	1131		1178	1134	14	3	17	9	νOC (41)
W(58)			1163	1119	2	0	6	4	βHCC(15) + νCC(11) + βHCC(15)
W(57)			1161	1117	87	16	14	8	βHCC(59)
W(56)	1095		1155	1111	353	66	3	2	βHCCO60)
W(55)			1088	1046	15	3	4	2	βHCC(17) + νCC(10)
W(54)			1078	1037	128	24	9	5	βHCH (81)
W(53)		1006	1064	1024	106	20	17	10	βHCH (74)
W(52)		994	1027	988	90	17	5	3	βHCH(74)
W(51)	971		1022	983	32	6	28	16	βHCH(86)
W(50)			1004	966	17	3	4	2	βOCC(45) + νOC(10)
W(49)			974	937	21	4	6	3	βCCC(30)
W(48)	910		950	914	4	1	1	0	νOC(18) + βCCC(10)
W(47)	874		904	870	15	3	1	1	βCCC(13) + νCC(13)
W(46)	840		868	835	25	5	7	4	βCCC(14)
W(45)			859	827	14	3	1	0	βCCC(14)
W(44)	810		839	807	91	17	1	1	βCCC(23)
W(43)			832	800	43	8	1	1	βCCO(10)
W(42)			822	791	117	22	0	0	βOCC(15) + βCCC(20)
W(41)	766	772	814	783	22	4	1	1	βCCC(22)
W(40)	740		764	735	23	4	33	18	βCOC(15)
W(39)			741	713	4	1	4	2	βOCC(48)
W(38)			732	704	10	2	2	1	βOCC(22) + βCCC(20)
W(37)	676		712	685	1	0	6	3	βOCC(35)
W(36)			673	648	2	0	2	1	βCCC(22)
W(35)	632	630	658	633	10	2	16	9	βCOC(62)
W(34)			653	628	3	1	2	1	βOCC(23)
W(33)			641	617	9	2	2	1	τHOCC(96)
W(32)			626	603	3	0	1	0	τHOCC(94)
W(31)	589	588	612	589	12	2	10	6	τHOCC(89)

(*continued on next page*)

Table 2 (*continued*)

Mode No	Experimental wave number (cm-1)		Theoretical wave number (cm-1)		IR intensities		RAMAN intensities		Assignments PED
	FTIR	FT RAMAN	Unscaled frequency	Scaled frequency	Rel	Abs	Rel	Abs	
W(30)			590	568	4	1	13	7	τHCCC(50)
W(29)	539		559	538	39	7	2	1	τHCCC(69)
W(28)			545	524	5	1	7	4	τHCCC(82)
W(27)			536	515	18	3	1	1	τHCCC(78)
W(26)			510	491	8	1	8	4	τHCCC(75)
W(25)			503	484	152	29	3	2	τHCOC(35) + βHCO(31) + νCC(11)
W(24)			478	460	15	3	0	0	τHCCC(16)
W(23)			468	451	14	3	0	0	ττHCCC(25)
W(22)			459	442	4	1	2	1	τHCOC(11) + βHCH (15)
W(21)			414	398	3	1	11	6	τHCOC(35) + βHCH (20)
W(20)			410	394	144	27	3	2	τCCCC(37)
W(19)			388	373	1	0	2	1	τCCCC(54)
W(18)		345	364	350	3	1	1	0	τCCCC(31) + τHCOC(12)
W(17)			348	335	13	2	0	0	τCCCC(55)
W(16)			300	288	0	0	1	0	τCCCC(13) + βCCC(14)
W(15)			297	286	1	0	1	1	τCCCC(55)
W(14)			263	253	2	0	3	1	τCCOC(10)
W(13)			244	234	4	1	2	1	τCOCC(51)
W(12)			233	224	1	0	1	0	τCCCC(13) + βCCC(26)
W(11)			226	217	0	0	1	0	τCOCC(13) + βOCC(10)
W(10)		212	224	215	0	0	0	0	τOCCC(78)
W(9)			178	171	2	0	4	2	τOCCC(21)
W(8)			165	159	2	0	1	1	τOCCC(47) + τCCCC(34)
W(7)			157	151	2	0	0	0	τOCCC(79)
W(6)			120	115	1	0	1	1	τOCCC(37)
W(5)			99	95	2	0	0	0	τOCCC(11) + βCCC (13) + βOCC(17)
W(4)		81	84	81	4	1	1	0	τCCCC(63)
W(3)			41	39	0	0	4	2	τCCCC(31)
W(2)			39	37	1	0	3	1	τCCCC(66)
W(1)			18	17	2	0	8	4	τCCCC(10)

1ν- Stretching, β-Bending, τ- Torsion.
2Scaling Factor 0.961 for B3LYP6-311G (d,p).
3Relative absorption intensity normalized with highest peak absorption equal to 100.
4Relative Raman intensity normalized to 100.

The FT-Raman spectrum was also recorded using 1064 nm line of Nd: YAG laser as excitation wavelength in the region 4000-100 cm^{-1}on a BRUKER model IFS 66 V spectrophotometer equipped with FRA 106 FT-Raman module accessory. The experimental and theoretically predicted FT-IR and FT-Raman spectra of Hesperetin with their scaled frequencies using scaling factors for each mode are compared.

4. Computational details

The entire calculations were performed at B3LYP (Becke 3-Lee-Yang and Parr) level of theories (Becke A.D., 1993; Parr R.G. et al., 1984) in Gaussian 09 program (Frisch, M.J. et al., 2009). The optimized structure was visualized by Gauss View 5.0 software (Raja, M., 2016). The optimized molecular structural parameters were used to determine the harmonic vibrational frequency. Vibrational wave numbers were computed using same level of theory and Chemcraft Program for the title molecule (G.A. Zhurko, 20004) and the potential energy distribution (PED) calculation is used to assign the Wavenumber for Hesperetin molecule using VEDA 4.0 program (Kereztury,G. et al., 1993; Jamroz, M.H., 2004). Scaling factors are used to obtain good confirmation with the experimental values has the calculation are done in gas phase. Frontier Molecular Orbitals (FMOs) and Molecular Electrostatic Potential (MEP) analysis (Rauhut, G., 1995; Mulliken,R.S., 1934; Murray,J.S. et al., 2011) was done using DFT/B3LYP method with 6-311G (d,p) basis set. Using the same level of theory, Fukui function, local softness and electrophilic indices were calculated from Mulliken atomic charge of Hesperetin molecule (Yang, W. et al., 1985). The total density of states (TDOS), overlap population density of states (OPDOS) and the partial density of states (PDOS) spectra were charted by using the program GaussSum 2.2 (O'Boyle, N.M. et al., 2008).The molecular docking studies were performed by AUTODOCK (1.4.6 version) program (Trott, O., & Olson, A.J., 2010). Hence docking plays a vital role in biological and pharmaceutical analysis of drug design and drug discovery. PyMOL (Delano, W.L., 2002), Chimera (Xin Liu et al., 2008) and Discovery studio programs were used to view the protein-ligand complex and the intermolecular interactions between protein and the ligand molecules.

5. Results and discussion

5.1. Geometrical structure

The optimized structural parameters of the Hesperetin were calculated at B3LYP levels with the 6-311G (d, p) basis set and are recorded in Table 1 in agreement with the atom numbering scheme as obtained from CHEMCRAFT software and represented in (Fig. 1). The computed parameters of bond length and bond angle are compared with experimental geometrical parameters (Shin, W. et al., 1987). The difference between theoretical and experimental geometry can generally be described in a way that calculations were performed utilizing isolated molecule in the gaseous phase to achieve theoretical results and in solid state for experimental results. The theoretical values for the Hesperetin molecule was found to be closely related to the experimental XRD values. Exactly matching bond length values were calculated for the C10-O22, are found to be 1.361 Å, (experimental) and 1.361 Å (theoretical), respectively. The calculated bond lengths C1-O6 (1.442 Å, 1.486 Å), C15-C16 (1.381 Å, 1.386 Å) are found to be slightly higher than the experimental values. This molecule has seventeen C-C bonds, seven C-O bonds and one O-C bond.

Table 3
Mulliken Charge Distribution, Fukui Function, Local Softness and Electrophilicity indices corresponding to (0,1), (−1,2) and (1,2) charge and multiplicity of Hesperetin.

Atoms	Mulliken Atomic Charges			Fukui Functions			Local Softness			Electrophilicity Indices		
	N (0,1)	N+1(-1,2)	N-1(1,2)	f^+r	f^-r	f^0r	S^+r	S^-r	S^0r	ω^+r	ω^-r	ω^0r
C1	0.0923	−0.0805	0.0877	−0.1728	0.0046	−0.0841	−0.0373	0.001	−0.0181	−0.2157	0.0058	−0.1049
C2	−0.2451	0.2893	−0.2074	0.5344	−0.0377	0.2483	0.1152	−0.0081	0.0535	0.6668	−0.047	0.3099
C3	0.3979	0.4120	0.3059	0.0141	0.0919	0.0530	0.0030	0.0198	0.0114	0.0176	0.1147	0.0661
C4	−0.0255	0.1832	−0.2622	0.2087	0.2367	0.2227	0.045	0.0510	0.0480	0.2604	0.2953	0.2779
C5	0.3281	−0.0347	0.24421	−0.3628	0.0839	−0.1394	−0.0782	0.0181	−0.0301	−0.4527	0.1047	−0.174
O6	−0.5501	−0.1140	−0.3543	0.4360	−0.1957	0.1201	0.0940	−0.0422	0.0259	0.5440	−0.2442	0.1499
C7	−0.2032	−0.1257	−0.0945	0.0774	−0.1087	−0.0156	0.0167	−0.0234	−0.0034	0.0966	−0.1357	−0.0195
C8	0.3515	0.5997	0.1866	0.2481	0.1649	0.2065	0.0535	0.0355	0.0445	0.3096	0.2058	0.2577
C9	−0.1405	−0.0738	−0.0475	0.0666	−0.0929	−0.0132	0.0143	−0.02	−0.0028	0.0831	−0.116	−0.0164
C10	0.3196	0.3947	0.2429	0.0751	0.0767	0.0759	0.0162	0.016	0.0163	0.0937	0.0957	0.0947
O11	−0.5493	−1.2134	−0.3483	−0.6641	−0.2010	−0.4326	−0.1432	−0.0433	−0.0933	−0.828	−0.2508	−0.5398
C12	0.0865	0.3738	−0.1699	0.2872	0.2565	0.2718	0.0619	0.0553	0.0586	0.3586	0.3200	0.3392
C13	−0.1311	0.0140	−0.0089	0.1451	−0.1221	0.0115	0.0312	−0.0263	0.0024	0.1810	−0.1524	0.0143
C14	0.2926	0.2131	0.1845	−0.0795	0.1081	0.0143	−0.0171	0.0233	0.0030	−0.0993	0.1349	0.0178
C15	0.3311	0.6458	0.1943	0.3146	0.1368	0.2257	0.0678	0.0295	0.0486	0.3926	0.1707	0.2817
C16	−0.1364	0.0119	−0.082	0.1483	−0.0544	0.0469	0.0319	−0.0117	0.0101	0.1850	−0.0679	0.0585
C17	−0.1402	−0.0552	−0.0222	0.0850	−0.1180	−0.0165	0.0183	−0.0254	−0.0035	0.1061	−0.1472	−0.0205
O18	−0.5594	−1.3445	−0.3564	−0.7851	−0.2031	−0.4941	−0.1693	−0.0438	−0.1065	−0.9796	−0.2534	−0.6165
C19	−0.0788	0.6889	−0.1368	0.7677	0.0579	0.4128	0.1655	0.0124	0.0890	0.9580	0.0723	0.5151
O20	−0.5656	−0.7611	−0.2745	−0.1956	−0.2911	−0.2433	−0.0422	−0.0628	−0.0525	−0.244	−0.3632	−0.3036
O21	−0.5479	−0.9865	−0.3127	−0.4386	−0.2351	−0.3369	−0.0946	−0.0507	−0.0726	−0.5473	−0.2934	−0.4204
O22	−0.5652	−0.9112	−0.2855	−0.3460	−0.2798	−0.3129	−0.0746	−0.0603	−0.0675	−0.4317	−0.3491	−0.3904
H23	0.1053	−0.0734	0.1748	−0.1787	−0.0695	−0.1241	−0.0385	−0.015	−0.0268	−0.223	−0.0867	−0.1549
H24	0.1356	−0.0295	0.1614	−0.1651	−0.0258	−0.0955	−0.0356	−0.0056	−0.0206	−0.206	−0.0323	−0.1191
H25	0.1443	−0.0486	0.1723	−0.1929	−0.0280	−0.1105	−0.0416	−0.006	−0.0238	−0.2407	−0.035	−0.1379
H26	0.0881	0.0195	0.1309	−0.0686	−0.0428	−0.0557	−0.0148	−0.0092	−0.012	−0.0855	−0.0534	−0.0695
H27	0.1070	0.0032	0.1579	−0.1038	−0.0509	−0.0774	−0.0224	−0.011	−0.0167	−0.1296	−0.0635	−0.0965
H28	0.1063	0.0437	0.1385	−0.0626	−0.0322	−0.0474	−0.0135	−0.0069	−0.0102	−0.0781	−0.0401	−0.0591
H29	0.0909	0.0361	0.1463	−0.0548	−0.0554	−0.0551	−0.0118	−0.0119	−0.0119	−0.0684	−0.0691	−0.0687
H30	0.0819	0.0280	0.1307	−0.0538	−0.0488	−0.0513	−0.0116	−0.0105	−0.0111	−0.0672	−0.0609	−0.0641
H31	0.1289	−0.0549	0.1682	−0.1838	−0.0393	−0.1115	−0.0396	−0.0085	−0.024	−0.2293	−0.049	−0.1392
H32	0.1198	−0.0578	0.1507	−0.1777	−0.0309	−0.1043	−0.0383	−0.0067	−0.0225	−0.2217	−0.0386	−0.1301
H33	0.1198	−0.0571	0.1507	−0.1769	−0.0309	−0.1039	−0.0381	−0.0067	−0.0224	−0.2207	−0.0386	−0.1297
H34	0.2885	0.3349	0.2851	0.0464	0.0034	0.0249	0.0100	0.0007	0.0053	0.0579	0.0042	0.0311
H35	0.2420	0.2507	0.2702	0.0086	−0.0282	−0.0098	0.0018	−0.0061	−0.0021	0.0108	−0.0352	−0.0122
H36	0.2286	0.4785	0.2786	0.2499	−0.0501	0.0999	0.0538	−0.0108	0.0215	0.3118	−0.0625	0.1247

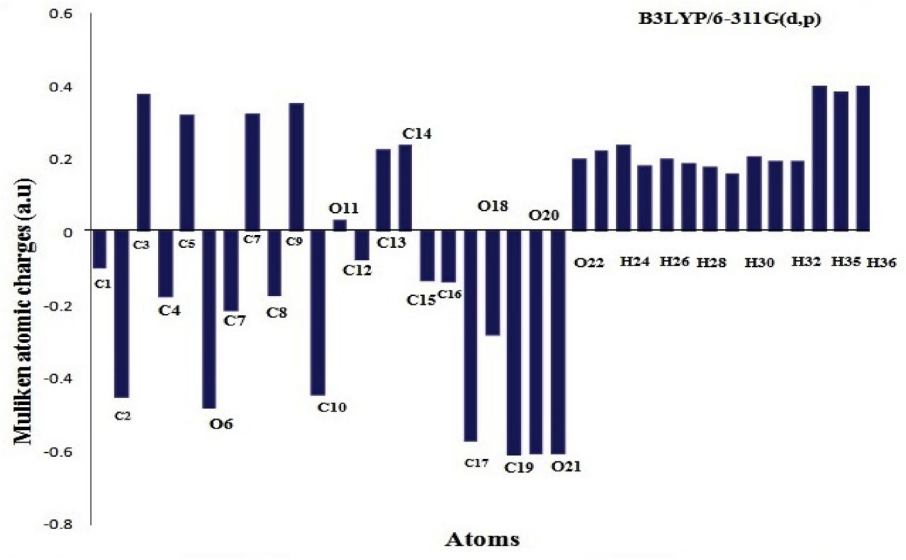

Fig. 3. The histogram of calculated Mulliken atomic charge of Hesperetin.

5.2. Vibrational analysis

The Hesperetin molecule consists of 36 atoms, assuming C_1 point group of symmetry and has 102 normal modes of vibrations. All the vibrations are active both in Raman and IR absorption spectra and are shown in (Fig. 2a and b) respectively. The measured (FTIR and FT-Raman) wave numbers and assigned wave numbers of some selected intense vibrational mode calculated at the B3LYP level with basis set 6-311G (d,p) along with their PED are presented in Table 2.

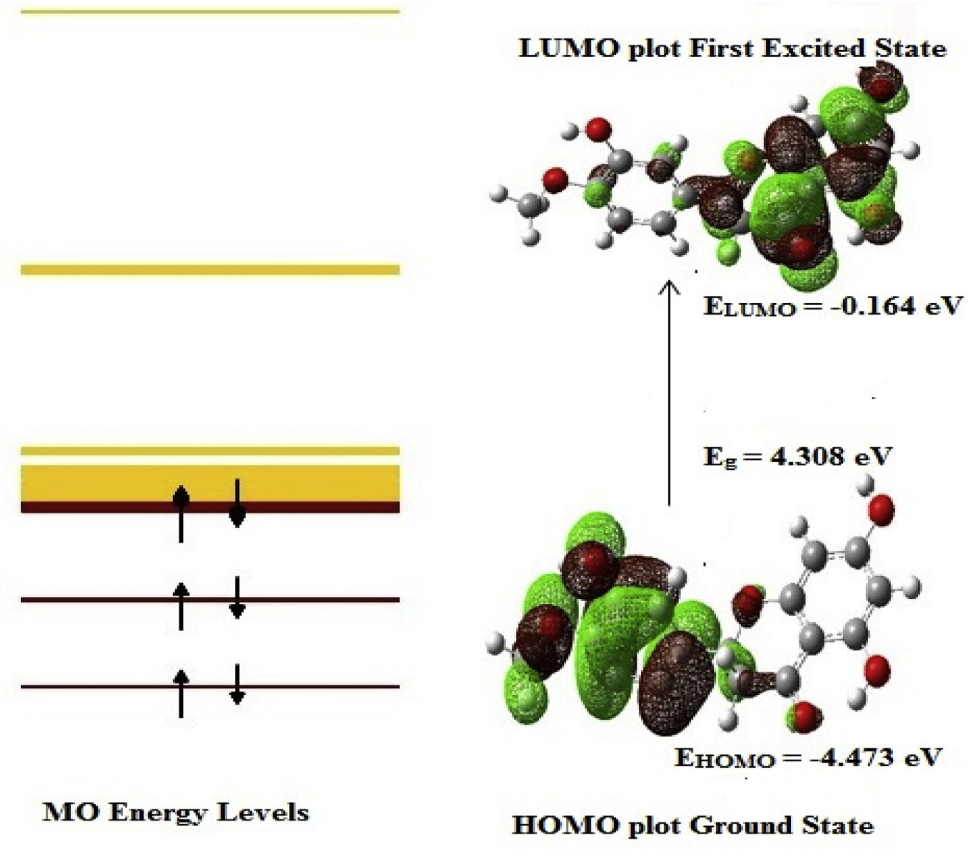

Fig. 4. The HOMO and LUMO orbitals of Hesperetin.

Table 4
Calculated global reactivity descriptors for Hesperetin.

Molecular descriptors energy (eV)	B3LYP/6-311G (d,p)
HOMO energy(E_{HOMO})	−4.4730
LUMO energy(E_{LUMO})	−0.1643
Energy gap (E_g)	4.3086
Ionization potential (I)	4.4730
Electron affinity(A)	0.1643
Chemical potential (μ)	−2.3187
Chemical Hardness (η)	2.1543
Chemical softness (S)	0.2156
Electronegativity (μ)	2.3187
Electrophilicity (ω)	1.2478

5.2.1. O-H vibrations

The hydroxyl stretching vibrations are generally (Muthu, S., & Jsac Paularj, E., .2012) observed in the region around 3000-3500 cm^{-1}. O-H stretching vibration is observed only in FTIR at 3427 cm^{-1} which occurs as a broadband. The hydroxyl vibration is supported by B3LYP/6-311G (d,p) method at 3558 cm^{-1}. This pure mode shows 100% PED contribution.

5.2.2. C-H vibrations

The aromatic C-H ring stretching vibrations are normally found in the region 3100-3000 cm^{-1} (Sarojini, K et al., 2013). The C-H stretching modes generally appear with Raman intensity and are highly polarized. In the theoretical frequency C-H stretching vibrations were observed in peaks at 3104 cm^{-1} to 2898 cm^{-1} FT-Raman spectrum and 3061 $cm^{-1}$to 2918 cm^{-1}in the FT-IR spectra. The peak corresponding to C-H stretching vibration are observed at the range of 3117 cm^{-1} to 2897 cm^{-1} in B3LYP/6-311G (d,p) method, shows good confirmation with recorded experimental spectral values. The PED corresponding to these vibrations are found to be in the range of 88–100%.

5.2.3. C-C vibrations

The aromatic ring vibrations give rise to attributed bands in peaks observed in both FTIR and FT-Raman spectra, covering the spectral range from 1600 to 1400 cm^{-1}(Muthu,S. et al., 2014). In the present work, the CC stretching vibration bands which are of different intensities were observed at 1609, 1518, 1444,1402 and 1294 cm^{-1} in FTIR spectrum and Raman bands were identified at 1563, 1485, 1464,1454,1301 and 1291 cm^{-1}. The theoretical values were obtained in the range of 1602 cm^{-1} to 1046 cm^{-1} by B3LYP6-311G (d,p) method. It shows that the theoretical values are in good agreement with the experimental data.

5.2.4. O-C vibrations

In the present work, O-C stretching vibrations are observed in the region 1260-1000 cm^{-1}(Muthu, S. et al., 2003). The peaks corresponding to O-C stretching vibration were observed in at 1344 to 1178 cm^{-1} in the theoretical method. Its supported well by the experimental intensity observed at 1294, 1204, 1184 and 1131 cm^{-1} in FTIR spectrum and at 1291, 1311 and 1187 cm-1 in the FT-Raman spectrum.

5.3. Fukui function

The electron density based on the local reactivity descriptors are used to predict the positive reactive sites of the molecule and it is important in designing the pharmaceutical compound. The Fukui function helps one to predict the most reactive site for electrophilic and nucleophilic attack within a molecule (Morell, C. et al., 2006; Ayers, P. et al., 2000). In the present study, the local descriptors such as Fukui (f_r^+, f_r^-, f_r^0), local softness (S_r^+, S_r^-, S_r^0) and electrophilicity indices (ω_r^+,

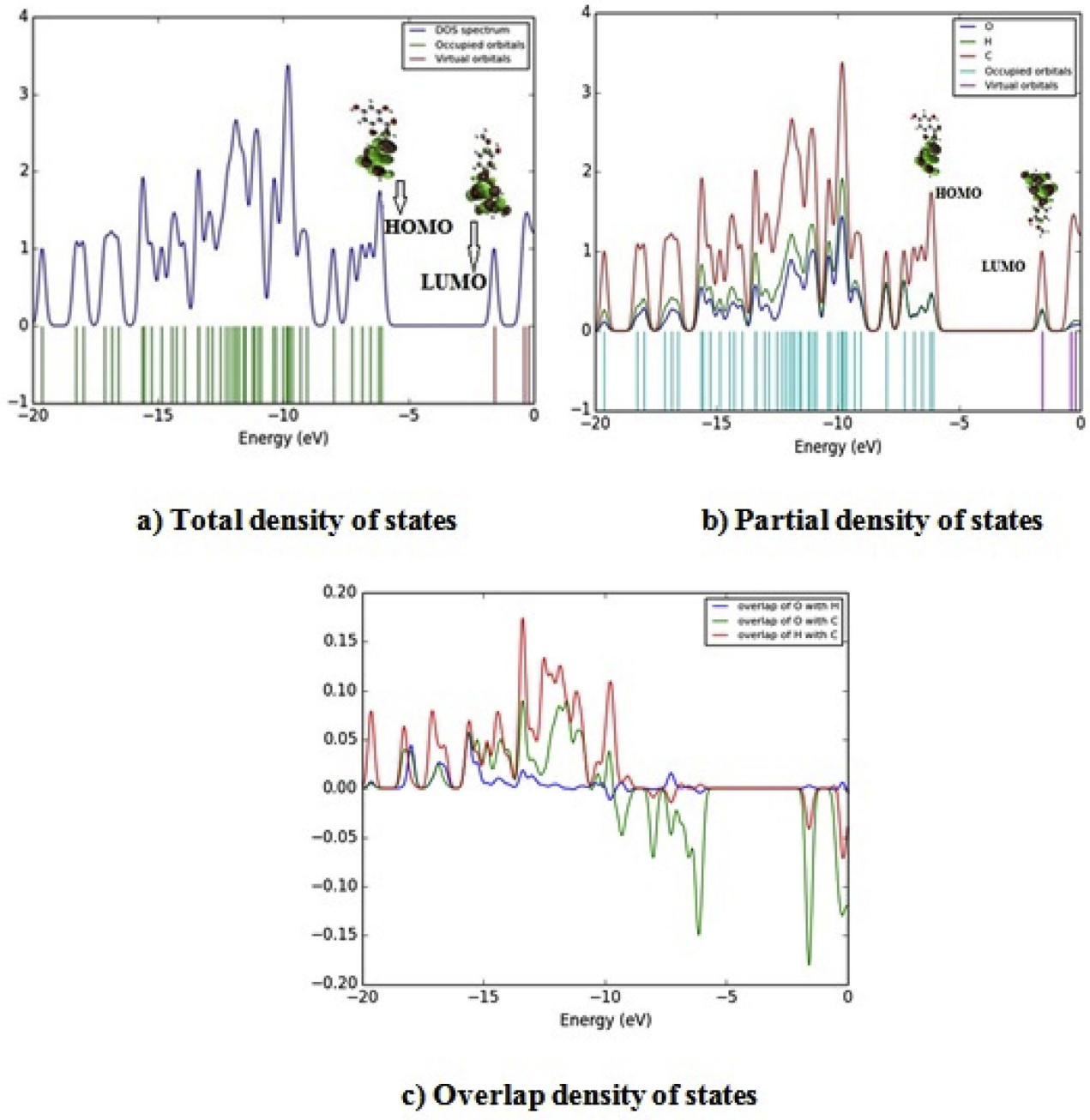

Fig. 5. a) Total, b) Partial and c) Overlap population density of states of Hesperetin.

ω_r^-, ω_r^0) were calculated for the Hesperetin molecule and are tabulated in Table 3.

$f_r^+ = q_r\ (N+1)\text{-}q_r\ (N)$

$f_r^- = q_r(N)\text{-}q_r(N\text{-}1)$

$f_r^0 = [q_r\ (N+1)\text{-}q_r(N\text{-}1)]/2$

In these equations, q_r is the atomic charge at the rth atomic site in the neutral (N), negatively charged (N+1), positively charged (N-1) chemical species (Chattaraj, P. et al., 2003). Fukui function shows the more reactive regions and leads to the chemical properties in a molecule. From the calculated values, the reactivity order for the nucleophilic case was C2 > O6 > C15 > C12 > H36 > C8 > C4 > C16 > C17 > H34 > H35, on the other hand electrophilic attack can be observed in the order O20 > O22 > O21 > C18 > O11.

5.4. Mulliken charge distribution

The natural population analysis of Hesperetin molecule is obtained by Mulliken (Mulliken, R.S., 1995) population analysis using B3LYP/6-311G (d,p) method. Due to the general utility of atomic charges, various methods have been developed for calculating them from quantum chemical wave functions (Sidir I. et al., 2010). Distribution of positive and negative charges is vital in increase or decrease of bond length between the atoms. Atomic charge affects dipole moment, polarizability, electronic structure and other molecular properties of the system. The results can be represented better in illustrated form as given (Fig. 3). Charge distribution of the Hesperetin Molecule shows that all the hydrogen atoms are positively charged whereas the magnitude of the atomic charges on carbon atoms were observed to be both positive and negative ranging from 0.3731 to −0.6179. From Fig. 3, we

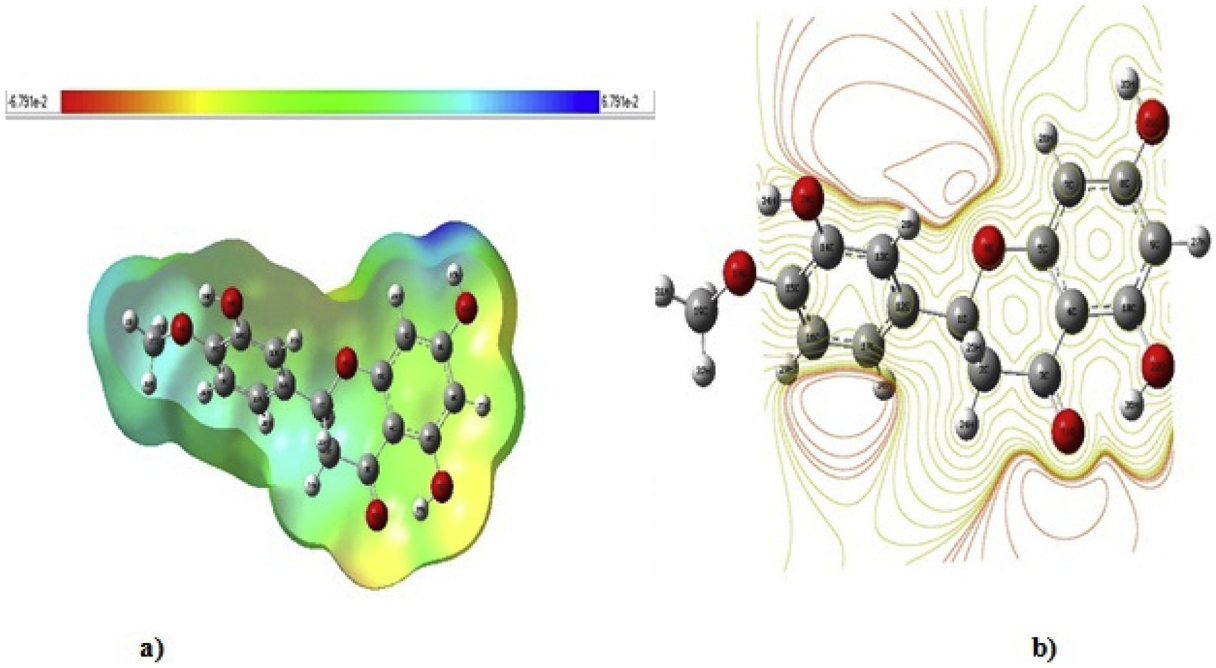

Fig. 6. a) Molecular Electrostatic potential map of Hesperetin molecule and b) The contour map of electrostatic potential of the total density of Hesperetin.

Table: 5
Thermodynamic properties for Hesperetin obtained by B3LYP/6-311G (d,p) method.

T (K)	S (J/mol.K)	Cp (J/mol.K)	H (kJ/mol)
100	371	124	8
200	487	222	25
298	593	317	52
300	595	318	52
400	699	406	88
500	798	480	133
600	891	539	184
700	978	587	240
800	1059	626	301
900	1135	658	365
1000	1205	685	432

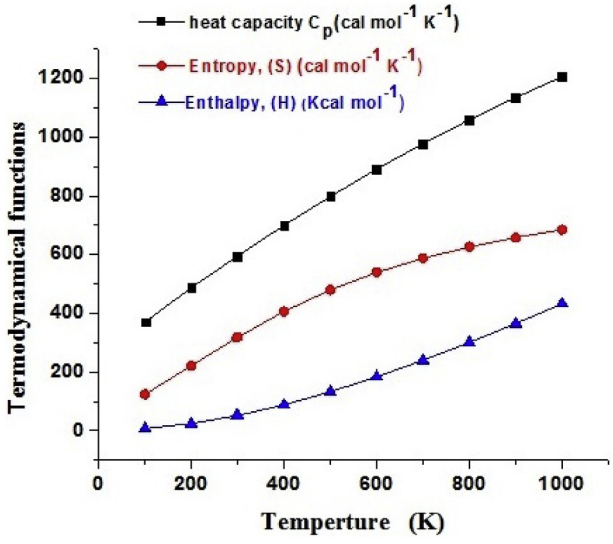

Fig. 7. Graphs representing dependence of Entropy, Heat capacity and Enthalpy on temperature of Hesperetin.

Table 6
ADMET data and drug likeness of Hesperetin.

A	B	C	D	E	F	G	H
302.27	90.9	0	2.14	Yes	Yes	Mutagen	0.222

A: Molecular Weight
B: ADMET Solubility (aqueous)
C: ADMET absorption level
D: ADMET_SK logP
E Lipniski's filter
F: Druglikeness, inference
G: Ames mutagenicity
H: ADMET_BBB

can see that the maximum atomic charges are obtained for O_{20} atom. In addition to this, all oxygen atoms exhibit negative charge.

5.5. Global reactivity descriptors

The concept of highest occupied molecular orbit (HOMO) and lowest unoccupied molecular orbit (LUMO) is an important tool as it helps to understand the chemical stability and reactivity of the molecule. The interaction of HOMO and LUMO results in the transition of electrons (Subramanian, N. et al., 2010). The pictorial representation of HOMO and LUMO for the Hesperetin is shown in (Fig. 4). The corresponding energy values and energy gap (ΔE) which explains the overall reactivity of the molecule is listed in Table 4. Further, the parameters like electronegativity, chemical potential, global hardness and softness were defined using the above mentioned energy values. They are related to each other using the following equations (Christina Susan Abraham, et al 2017). The calculated band gap value 4.3086eV indicates that the Hesperetin molecule has a stable structure. The Hesperetin molecule has a lower softness value of 0.2156. The softness value helps in understanding the toxicity of various pollutants in terms of their reactivity and site selectivity. The higher hardness and lower softness value indicates the stability of the molecule. The lower chemical potential and electrophilicity index values reveal that the title compound potentially bioactive molecule.

Table 7
Hydrogen bonding and molecular docking with protein targets for Hesperetin.

Protein PDB ID	Bonded residues	Bond distance (Å)	Estimated inhibition constant	Binding energy Kcal/mol	Intermolecular energy Kcal/mol	Reference RMSD (Å)
3O96	Gln79 Thr211 Leu210	2.2 2.0 2.4	33.58	−6.10	−7.60	12.83

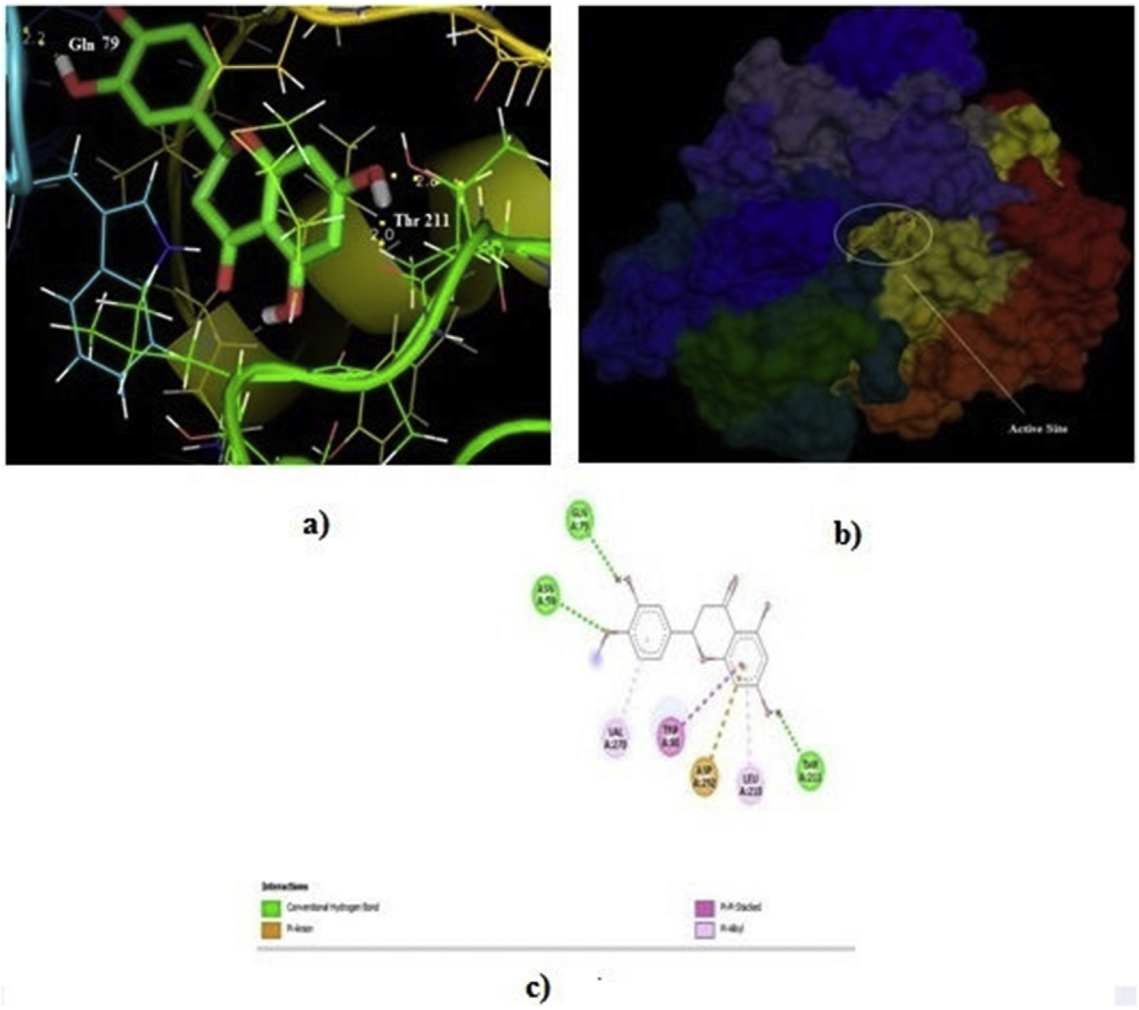

Fig. 8. Hesperetin docked into the binding site (2D, 3D) of PI3K/AKT Inhibitor.

5.6. Density-of-states (DOS)

As a reasonable explanation of the frontier orbitals cannot be obtained by simply analyzing HOMO-LUMO, TDOS, OPDOS and PDOS spectra are employed and plotted with energies on the X-axis and the calculated respective density values on the Y-axis (Hughbanks T., 1983; Malecki J.G., 2010; Pople J.A. et al., 1993) using GaussSum 2.2 software. The occupied and virtual levels are clearly indicated in the TDOS plot, which provides the molecular orbital composition with respect to their chemical bonding. The OPDOS plot determines the donor-acceptor properties of the ligands and bonding and non-bonding interactions. The overlap of hydrogen with carbon exhibits a positive value, which clearly indicates the bonding interaction of hydrogen atoms. The bonding nature of carbon atoms with hydrogen atoms is much higher (because of positive overlap population).Since it is very difficult to compare groups in terms of their bonding and anti-bonding properties, the PDOS spectrais plotted and the spectras corresponding to density of states are shown in (Fig. 5a–c). The PDOS plot mainly presents the composition of the fragmented orbitals contributing to the molecular orbitals. The HOMO levels are localized on the ring, and their subscriptions are about 90% and the LUMO orbitals are localized on the ring and their subscriptions are 75% of the compound.

5.7. 7Molecular Electrostatic potential

MEP is an important tool for analyzing the active binding site of the molecule by colour grading and to predict the interaction of the reactive site of a molecule (Singh, S. et al., 2017; Okulik, N. et al., 2005). Using Gauss view 5.0 software B3LYP/6-311G (d,p) method MEP surface and contour map is drawn for the Hesperetin molecule as shown in (Fig. 6a and b).The colour code of these maps ranges from -6.791×10^{-2} to 6.791×10^{2} eV, where Blue indicates the strongest attraction and red indicates repulsion. The electrophilic reactivity is indicated by the red region of the MEP and the nucleophilic reactivity by the blue region. For the Hesperetin molecule negative regions are mainly localized over nitrogen atoms, which are the most reactive sites

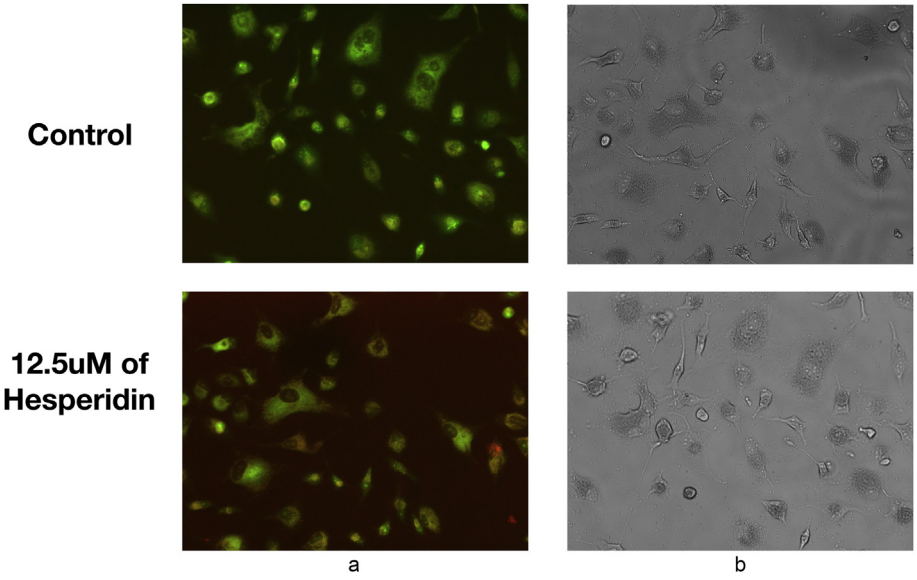

Fig. 9. Morphological changes of A549 cells under fluorescence microscope (EB/AO staining, 40x).

for electrophilic attack whereas the positive regions are around hydrogen atoms, which are the most reactive sites for nucleophilic attack. Thus MEP is a very useful tool for giving information about intermolecular interactions.

5.8. Thermodynamic properties

The standard statistical thermodynamic parameters like Heat capacity (C), Entropy (S) and Enthalpy (H) for the Hesperetin molecule were computed for a range of temperature from 100 K to 1000 K on the basis of vibrational analysis at B3LYP/6-311G(d,p) level and the values are listed in Table 5. The thermodynamic function increases with increasing temperature due to the fact that the molecular vibrational intensities increase with temperature, along with the increase in translational and rotational energy in accordance with the equipartition theorem (Shoba, D. et al., 2014).The linear and quadratic formulas are used to fit the correlation equations between thermodynamic functions and temperatures. The corresponding fitting factors (R^2) for these thermodynamic properties are 0.99963, 1.0000 and 0.99928, respectively. The corresponding fitting equations are as follows and the correlation graph is shown in (Fig. 7).

$$C_P = 7.50632 + 1.19832T–5.24993 \times 10^{-4} T^2 \ (R^2 = 0.99963)$$

$$S = 250.34004 + 1.23586T - 2.8098 \times 10^{-4} T^2 \ (R^2 = 1.0000)$$

$$H = -14.99739 + 0.14217–3.1008 \times 10^{-4} T^2 \ (R^2 = 0.99928)$$

All thermodynamic data provide useful information for further studies. To calculate the other thermodynamic energies in accordance to relationships of thermodynamic functions and estimate directions of chemical reactions according to the second law of thermodynamics in thermochemical field (Zhang, R. et al., 2010).

5.9. Drug-likeness and ADMET prediction

Drug likeness of the molecule was investigated using Lipinski rule of five (Lipinski, C.A et al., 1997). Also, the toxicity was predicted under the Calculated Molecular Property module of Small molecule tool and the results were summarized in Table 6." *Lipinski's rule states that poor absorption is anticipated if the molecular weight is greater than 500; log P greater than 5*"(Lipinski, C.A et al., 1997). The Hesperetin molecule satisfies the Lipinski's rule which indicates that the molecule is qualified to be a drug and is presented in Table 6. The ADMET prediction for a drug is the combination of five operations (Absorption, Distribution, Metabolism, Excretion and Toxicity) which the title compound undergoes while given orally to a patient. The calculated ADMET properties show that the title compound can be used as an effective drug in future.

6. Molecular docking

The molecular docking study was carried out for Hesperetin (Sledz, P. et al., 2018). In drug discovery to reduce the time and cost and increase the efficiency of the medicine Molecular Docking method has been used. It is a current technique to get insight study of the exact binding location of the ligand and protein (Kragh-Hansen, U 1981). In this study, we can understand the transport of small molecule called ligand in biological systems. The molecular modelling is used to predict the ideal binding orientation, affinity and activity of drug molecules and their protein targets which have the properties of AKT/PI3 Kinase inhibitor (PDB ID: 3O96) (Wen-I Wu. et al., 2010) downloaded from RCSB from the PDB format. The ligand was docked in the functional sites of the selected protein and minimum binding energy value was examined. Docked conformation which had the lowest binding energy was chosen to study the mode of binding. The docking parameters of binding energy, Reference RMSD (Å), inhibition constant and intermolecular energy of the molecule with respect to the targeted protein were computed and tabulated in Table 7. The binding orientation of Hesperetin with targeted protein is shown in (Fig. 8). The dotted yellow lines show the formation of hydrogen bonds between the targeted protein and ligand. The minimum binding energy of −6.10 kcal/mol and intermolecular energy of −7.60 kcal/mol were seen in the interaction. This protein has three residues hydrogen bond having such as Gln79, Thr211 and Leu210 with bond distance 2.2, 2.0 and 2.4 Å. This lower binding energy shows that the PI3K Inhibitors (3O96) is properly bound with Hesperetin.

6.1. Inhibitory effects of hesperetin on the growth of A549 lung cancer cells

The cells underwent marked morphological changes such as becoming round in shape and apoptotic bodies were observed (Fig. 9b) by treatment with 12.5 μM of Hesperetin, compared with the untreated control. Fluorescence microscopy morphological changes of ethidium bromide/acridine orange stained A549 cells (Fig. 9a) showed that the percentage of apoptotic cells after treatment with 12.5 μM and 25 μM of Hesperetin increased drastically to 21%.

7. Conclusion

The vibrational assignments and spectra of FT-IR and FT-Raman were recorded for Hesperetin has been proposed, aided by the DFT/B3LYP method using 6-311G (d,p) basis set. The geometrical parameters of bond length and bond angle were calculated using same level of theory and compared with the experimental data. The HOMO-LUMO and MEP studies revealed the active site of the molecule. The Fukui functions and TDOS, OPDOS were also determined. The thermo-dynamic functions of the molecule at different temperatures have been calculated. The heat capacity, entropy and enthalpy increased with increase in temperature owing to the intensities of the molecular vibrations. Drug-likeness filters such as ADMET and Lipinski's rule of five proposed that Hesperetin molecule have good biological reactivity.

Invivo study has been carried out to study the cytotoxicity and anti-proliferative effect of Hesperetin towards human lung cancer cells (A549) which revealed that Hesperetin drug can be used against gene activated lung cancer. Molecular docking analysis was carried out to explore the Lung cancer activity of the Hesperetin molecule. Docking studies of the Hesperetin with PI3K/AKT Kinase showed that this ligand is good molecule which docks well with AKT target. Therefore, Hesperetin molecule plays an important role in inhibiting the PI3K/AKT Kinase to regulate the lung cancer.

References

Abraham, Christina Susan, Prasana, Johanan Christian, Muthu, S., 2017. Quantum mechanical, spectroscopic and docking studies of 2-Amino-3-bromo-5-nitropyridine by Density Functional Method. Spectrochim. Acta, Part A 181, 153–163.

Arcaro, A., Guerreiro, A.S., 2007. The phosphoinositide 3-kinase pathway in human cancer: genetic alterations and therapeutic implications. Curr. Genom. 8, 271–306.

Ayers, P.W., Parr, R., Parr, G., 2000. Variational principals for describing chemicalreactions: the Fukui function and chemical hardness revisted. J. Am. Chem. Soc. 122, 2010–2018.

Becke, A.D., 1993. Density-functional thermochemistry. III. The role of exact exchange. J. Chem. Phys. 98, 5648–5652.

Burgering, B.M., Coffer, P.J., 1995. Protein kinase B (c-Akt) in phosphatidylinositol- 3-OH kinase signal transduction. Nature 376, 599–602.

Chan, T.O., Rittenhouse, S.E., Tsichlis, P.N., 1999. AKT/PKB and other D3 phosphoinositide-regulated kinases: kinase activation by phosphoinositide-dependent phosphorylation. Annu. Rev. Biochem. 68, 965–1014.

Chattaraj, P., Maiti, K., Sarkar, B., 2003. A unified treatment of chemicalreactivity and selectivity. J. Phys. Chem. A 107, 4973–4975.

Delano, W.L., 2002. PyMol Molecular Graphics System. Delano Scientific, San Carlos, CA, USA.

Frisch, M.J., Trucks, G.W., Schlegel, H.B., Scuseria, G.E., Ortiz, J.V., Cioslowski, J., Fox, D.J., 2009. Gaussian 09, Revision E.01. Gaussian, Inc., Wallingford CT.

Hughbanks, T., Hoffmann, R., 1983. J. Am. Chem. Soc. 105, 35 28.

Jamroz, M.H., 2004. Vibrational Energy Distribution Analysis, vol. 4 VEDA, Warsaw.

Jemal, A., Bray, F., Center, M.M., Ferlay, J., Ward, E., Forman, D., 2011. Global cancer statistics. Ca - Cancer J. Clin. 61, 69–90.

Kereztury, G., Holly, S., Varga, J., Besenyei, G., Wang, A.Y., During, J.R., 1993. Vibrational spectra of monothiocarbomates-ii. IR and Raman spectra, vibrational assignment, conformational analysis and ab initio calculations of S-methyl-N,Ndimethylthio carbamate. Spectrochim. Acta 49, 2007–2026.

Kragh-Hansen, U., 1981. Molecular aspects of ligand binding to serum albumin. Pharmacol. Rev. 33, 17–53.

Lewinsohn, E., Britsch, L., Mazur, Y., Gressel, J., 1989. Flavanone Glycoside Biosynthesis in Citrus: Chalcone Synthase, UDP-Glucose:Flavanone-7-O-Glucosyl-Transferase and -Rhamnosyl-Transferase Activities in Cell-free Extracts, vol. 91. pp. 1323–1328.

Lipinski, C.A., Lombardo, F., Dominy, B.W., 1997. Experimental and computational approaches to estimate solubility and permeability in drug discovery and development setting. Adv. Drug Deliv. Rev. 23, 3–25.

Liu, W., Li, J., Roth, R.A., 1999. Heregulin regulation of Akt/protein kinase B in breast cancer cells. Biochem. Biophys. Res. Commun. 261, 897–903.

Liu, Xin, et al., 2008. The structural basis of protein acetylation by the p300/CBP transcriptional coactivator. Nat. Lett. 451, 846–850.

Malecki, J.G., 2010. Polyhedron 29, 19–73.

Morell, C., Grand, A., Labbe, A.T., 2006. Theoretical support for using the Df(r) descriptor. J. Chem. Phys. Let. 425, 342–346.

Mulliken, R.S., 1934. A new electroaffinity scale; Together with Data on valence states and on valence ionization potentials and electron affinities. J. Chem. Phys. 2, 782–793.

Mulliken, R.S., 1995. Electronic population analysis on LCAO–MO molecular wave functions . I. J. Chem. Phys. 23, 1833–1840.

Murray, J.S., Politzer, P., 2011. The Electrostatic Potential: an Overview, vol. 1. Wiley Interdiscip Rev, pp. 153–163.

Muthu, S., Isa c Psulraj, E., 2003. Spectroscopic and molecular structure (monomeric and structure) investigation of 2-[2-hydroxyphenyl) carbonyloxy] benzoic acid by DFT method: a combined experimental and theoretical study. J. Mol. Struct. 1038, 145–162.

Muthu, S., IsacPaularj, E., 2012. Solid State Sci. 14, 476–487.

Muthu, S., Ramachandran, G., lascPaulraj, E., Swaminathan, T., 2014. Spectrochim. Acta A. 128, 603–613.

Muthuswamy, S.K., Gilman, M., Brugge, J.S., 1999. Controlled dimerization of ErbB receptors provides evidence for differential signaling by homo- and heterodimers. MCB (Mol. Cell. Biol.) 19, 6845–6857.

O'Boyle, N.M., Tenderholt, A.L., Langner, K.M., 2008. J. Comput. Chem. 29, 839–845.

Okulik, N., Jubert, A.H., 2005. Theoretical analysis of the reactive sites of non-steroidal Anti-inflammatory drugs, internet electronic. J. Mol. Des. 4, 17–30.

Parr, R.G., Yang, W., 1984. Density functional approach to the frontier-electron theory of chemical reactivity. J. Am. Chem. Soc. 106, 4049–4050.

Peyrou, M., Bourgoin, L., Foti, M., 2010. PTEN in non-alcoholic fatty liver disease/non-alcoholic steatohepatitis and cancer. Dig. Dis. 28, 236–246.

Pople, J.A., Scott, A.P., Wong, M.W., Radom, L., 1993. Isr. J. Chem. 33, 3–45.

Raja, M., Raj Muhamed, R., Muthu, S., Suresh, M., 2016. , Synthesis, spectroscopy (FT-IR,FT- Raman, NMR, UV-Visible), first order hyperpolarizability, NBO and molecular docking study of (E)-1-(4-bromobenzylidene)semicarbazide. J. Mol. Struct. 1128, 481–492.

Rauhut, G., pulay, P., 1995. Transferable scaling factors for density functional derivedvibrational force fields. J. Phys. Chem. 99, 3093–3100.

Sarojini, K., Krishnan, H., Kanakan, C.C., Muthu, S., 2013. Synthesis, structural, spectroscopic studies, NLO and HOMO-LUMO of 4-methyl-N-(3-nitrophenyl) benzene sulphonamide with experimental and theoretical approachs. Spectrochim. Acta 108, 159–170.

Shi, Y., Liu, X., Han, E.K., Guan, R., Shoemaker, A.R., Oleksijew, A., Woods, K.W., Fisher, J.P., Klinghofer, V., Lasko, L., 2005. Optimal classes of chemotherapeutic agents sensitized by specific small-molecule inhibitors of akt in vitro and in vivo. Neoplasia 7, 992–1000.

Shin, W., Kim, S., Chun, K.S., 1987. Structure of (R,S)-hesperetin monohydrate. J Acta cryst 43, 1946–1949.

Shoba, D., Periandy, S., Boomadevi, S., Ramalingam, S., Fereyduni, E., 2014. Spectrochim. Acta 118, 438–447.

Sidir, I., Sidir, Y.G., Kumalar, M., Tasal, E., 2010. Ab intio Hartree-Fock and density functional theory investigation on the conformational stability, molecular structure and vibrational spectra of 7- acetoxy-6-(2,3-dibromopropyl)-4,8-dimethylcoumarin molecule. J. Mol. Struct. 964, 134–151.

Singh, S., Singh, H., Karthick, T., Tandon, P., Dethe, D.H., Erande, R.D., 2017. Conformational study and vibrational spectroscopic (FT-IR and FT-Raman) analysis of an alkaloid- borreverine derivative. Anal. Sci. 33, 99–104.

Sledz, P., Caflish, A., 2018. Protein structure-based drug design: from docking to molecular dynamics. J. Struct. Biol. 48, 93–102.

Subramanian, N., Sundarganesan, N., Jayabharathi, 2010. Molecular structure, spectroscopic(FT-IR, FT-Raman, NMR, UV) studies and first-order molecular hyperpolarizabilities of 1,2-bis(3-methoxy-4-hydroxybenzylidene)hydrazine by density functional method. Spectrochim. Acta, Part A 76, 259–269.

Trott, O., Olson, A.J., 2010. Autodock vina, Improving the speed and accuracy of docking with a new scoring function, efficient optimization and multithreading. J. Comput. Chem. 31, 455–461.

Weichhart, T., Saemann, M.D., 2008. The PI3K/Akt/mTOR path- ¨ way in innate immune cells: emerging therapeutic applications. Ann. Rheum. Dis. 67, 70–74.

Wu, Wen-I., Walter, C., Voegtli, W.C., Sturgis, H.L., Dizon, F.P., Vigers, G.P., Brandhuber, B.J., 2010. Crytal Structure of Human AKT1 with an Allosteric Reveals a New Mode of Kinase Inhibition, vol. 5. pp. 12913 -12913.

Yang, W., Parr, R.G., 1985. Hardness, softness, and the fukui function in the electronic theory of metals and catalysis. Proc. Natl. Acad. Sci. U.S.A. 82, 6723–6726.

Zhang, R., Dub, B., Sun, Y., Sun, G., 2010. Spectrochim. Acta 75, 1115–1124.

Zhurko, G.A., Zhurko, D.A., 2004. Chemcraft Program. Academic Version 1.5.